Rigorous Modeling of UV Absorption by TiO_2 Films in a Photocatalytic Reactor

Z. Zhang, W. A. Anderson, M. Moo-Young
Dept. of Chemical Engineering, University of Waterloo, Waterloo, Ont., Canada N2L 3G1

The radiation absorption profiles on the surfaces of TiO_2 films in a corrugated-plate photocatalytic reactor were modeled based on first principles. A new term, the local-area-specific rate of energy absorption (LASREA), was adopted to describe the catalyst surface radiation in heterogeneous photoreactors. The LASREA and the energy absorption efficiency were both quite sensitive to the dimensions of the corrugated plates. Due to the multiple photon reflections between the opposing surfaces, corrugated plates possess a superior capability for recapturing longer wavelength photons that would otherwise be reflected out of some reactor designs. This results in higher energy absorption efficiency and more uniform LASREA on the catalyst films. Compared to a flat plate, corrugations are predicted to enhance the energy absorption efficiency by up to 50% for UV-A fluorescent-lamp-powered systems and more than 100% for solar-powered systems.

Introduction

As a potential water-treatment technology, photocatalysis has been extensively studied during the last two decades. In this process an oxide semiconductor, usually TiO_2, is photoexcited upon absorbing photons with appropriate energy levels. The photoexcited semiconductor produces electrons and holes (that is, electron vacancies) that can migrate to the solid surface and initiate a series of oxidation and reduction reactions that can simultaneously oxidize toxic organic water pollutants (Matthews, 1987), kill microorganisms (Belhacova et al., 1999), and/or reduce the valence of dissolved metal ions (Aguado et al., 1991). Photocatalysis has been explored for potential use in soil remediation (Holden et al., 1993), drinking-water purification (Lawton et al., 1999), industrial water (Lin and Rajeshwar, 1997) and groundwater (Mehos and Turchi, 1993) detoxification, and removing inhibition to biodegradation (Bolduc and Anderson, 1997). Reports on the degradation of different substances, reaction mechanisms and kinetics, activities of different catalysts, and effects of selected environmental conditions are abundant.

Despite the profuse work on the photochemical process and areas of potential applications, a similar research effort has not been reported on the related engineering issues. There is still a shortage of studies on the design and scale-up of photocatalytic reactors based on radiative and reactor performance models. Of the limited number of reactor-engineering-related publications, radiation fields were modeled rigorously in only a few studies (Romero et al., 1997; Pasquali et al., 1996; Cabrera et al., 1994; Marinangeli and Ollis, 1977). The effect of the recapture of reflected photons on the radiation absorption of an immobilized catalyst film has not yet been reported.

Radiative transfer in absorbing, reacting, and scattering reaction media has been properly described by a set of integral-differential equations (Cassano et al., 1995). A heterogeneous medium may be regarded as optically homogeneous provided that the smallest inhomogeneities are sufficiently small compared to the wavelength of the photon. The radiation fields in (pseudo)homogeneous photoreactors have been described using the local volumetric rate of energy absorption (LVREA) and modeled with the Lambert-Beer's law (Rizzuti, 1985) and the principles of geometric optics (Roger and Villermaux, 1979). However, the LVREA is not appropriate for describing the radiation absorption profiles on immobilized catalyst films.

In this work, a new term, the local-area-specific rate of energy absorption (LASREA), was adopted to characterize

Correspondence concerning this article should be addressed to W. A. Anderson.

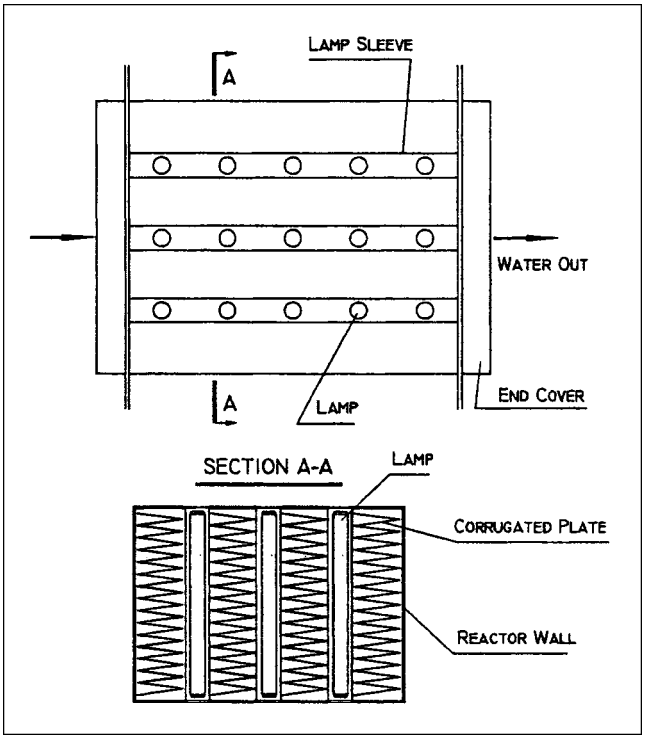

Figure 1. Corrugated-plate reactor: top view and cross-sectional view.

The water flows through the long triangular channels formed by the corrugations and the lamp sleeves, shown in Section A-A. The photocatalyst is immobilized on the surface of the corrugations and illuminated by the lamps. For solar illumination, only one corrugated plate would be illuminated on the one side pointed at the sun.

the radiation absorption profiles in heterogeneous photoreactors. The LASREA on the surfaces of the TiO_2 films in a corrugated-plate photocatalytic reactor was modeled based on the principles of geometric optics, the absorption and reflection characteristics of the catalyst film, and the refraction properties of the reaction medium and reactor components. Effects of the radiation sources, the photon recapture through multiple reflection, and the geometry of the catalyst support were considered.

Equipment and Materials

A lamp-illuminated corrugated-plate photocatalytic reactor is presented in Figure 1. The catalyst can be immobilized on both sides of the corrugated plates in this type of system, although only one layer of the corrugated plates could be directly illuminated in solar-powered systems. For the purpose of model development, a single corrugation (triangular channel) is taken from Figure 1 and placed in a rectangular coordinate system, as shown in Figure 2a. The height and length of the corrugated plate, B and L in Figure 2, were kept constant at 0.05 m and 0.5 m, respectively, during the simulation. The effect of the angle of the corrugated plate was examined numerically. The lamp sleeve properties were based on an ultraviolet-light (UV)-transmitting Plexiglas (G-UVT) sheet with a thickness of 6.35 mm. Two types of radiation sources were considered, UV-A fluorescent lamps (with emission characteristics similar to Philips TLK 40W/10R lamps, Philips Lighting Company, 1998) and solar UV.

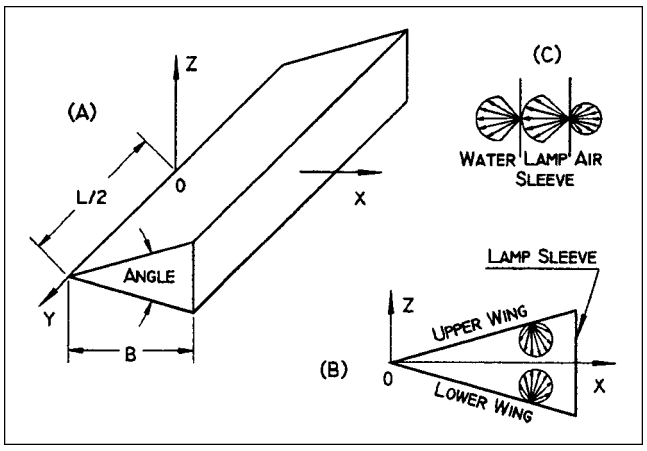

Figure 2. Coordinate system (a), (b) and radiation patterns due to reflection (b) and due to incidence and refraction (c).

Assumptions

The following assumptions were made in developing and applying the radiation model:

1. Photons from the lamps fall incident on the lamp sleeve in a diffuse way, as shown in Figure 2c. This assumption should be close to the real situation, since diffuse emission models have been found to be suitable for modeling fluorescent lamps (Alfano et al., 1986). The total irradiance on the surface of the lamp sleeve was assumed to be 120 $W \cdot m^{-2}$, based on measurements in experimental systems (Zhang, 1999).

2. In the UV-A range, solar UV possesses an irradiance with a direct parallel portion of 20 $W \cdot m^{-2}$ and a diffuse portion of 10 $W \cdot m^{-2}$. As is depicted in Figure A1 in the Appendix, the spectral irradiance increases linearly with the wavelength, being zero at 300 nm and reaching a maximum at 390 nm (Goswami, 1997; Curcó et al., 1996; Turchi and Mehos, 1994). In the modeling reported here, the sun's rays are assumed to be normal to the surface of the reactor cover (lamp sleeve).

3. The transmittance loss in the acrylic lamp sleeve is due entirely to extinction in the solid material. Photons are considered lost once they are reflected back to the lamp sleeve from the catalyst film. Reflections from the oppositely facing corrugated plate (Section A-A of Figure 1) are assumed to be insignificant.

4. Photons hitting the TiO_2 film will be subject to either absorption or coherent reflection in a diffuse way, as shown in Figure 2c. This should be a reasonable approximation since the immobilized catalyst film was found to be opaque to UV-A and optically rough (Zhang, 1999).

5. The spectral absorption coefficients of the TiO_2 film agree with the relevant information found in a previous work (Crittenden et al., 1995), as plotted in Figure A2 of the Appendix.

6. Within the UV-A range, the refractive index of the acrylic lamp sleeve was assumed to be constant at 1.49, based on relevant information from the literature (U.S. Precision Lens, 1973). The reaction medium was assumed to have a refractive index of 1.33, the same as that of water. The reaction medium was assumed to not significantly absorb in the wavelength range of interest.

Model Equations

Specific spectral irradiance on the lamp sleeve and the plates was calculated based on the assumed diffuse radiation pattern, the spectral irradiance of the lamps as provided by the supplier (Figure A1 in the Appendix), and the irradiance measured with a radiometer in experimental systems. The spectral extinction coefficients of the lamp sleeve (Figure A2 in the Appendix) were determined from first principles based on the refractive index and the spectral UV transmittance of this material, the diffuse radiation pattern, and energy balances within a unit hemisphere. The radiative energy profiles on the surfaces of the catalyst films were derived using the principles of geometric optics and analytical geometry through integration over the surfaces of the radiator (that is, the lamp sleeve), the reflector (that is, conjugate wings of the corrugated plate), and the wavelength distribution of the photons. A detailed derivation of the radiation model is provided in the Appendix.

Based on the coordinate system in Figure 2, the spectral local-area-specific rate of energy incidence on any point of the upper wing of the corrugated plate $P'(x', y', z')$, due to radiation from the lamp sleeve, is presented in Eq. 1.

$$I_u^s(y', z') = \frac{w_\lambda}{\pi}\left(\frac{n_w}{n_a}\right)^2 \iint_{S1} \frac{\cos\psi_1}{d_1^2}\cos\psi_w \times \exp^{(-k_3\delta[1-(n_w/n_p\sin\psi_w)^2]^{-0.5}-k_4 d_1)} dy\,dz. \quad (1)$$

In Equation 1, surface "$S1$" represents the region on the lamp sleeve that illuminates point $P'(x', y', z')$ of the upper wing. It can mathematically be expressed as: $n_w/n_a \sin\psi_w \le 1$.

Equation 2 shows the relationship between the incident and the absorbed energy at wavelength λ, for the case where the fluid between the lamp sleeve and catalytic surface is nonabsorbing in the UV-A range of interest:

$$q_u^s(y', z') = a(\lambda) I_u^s(y', z'). \quad (2)$$

Equation 3 is valid since the radiation field of the upper and lower wings of the corrugated plate are symmetric to plane $z = 0$:

$$I_u^s(y', z') = I_l^s(y', -z'). \quad (3)$$

Equation 4 gives the spectral local area-specific rate of energy incidence on the upper wing (point x', y', z') due to the first reflection from the lower wing:

$$I_u^{(1)}(y', z') = \frac{[1-a(\lambda)]}{\pi} \iint_{l} \frac{I_u^s(y, -z)\cos\psi_4\cos\psi_5}{d_2^2} \times \exp^{-k_4 d_2} dy\,dz \quad (4)$$

In Eqs. 1 and 4,

$$d_1^2 = (z'\cot\alpha - B)^2 + (y' - y)^2 + (z' - z)^2,$$

$$d_2^2 = [\cot\alpha(z' + z)]^2 + (y' - y)^2 + (z' - z)^2,$$

$$\cos\psi_1 = \sin\alpha(B - z\cot\alpha)/d_1,$$

$$\cos\psi_w = (B - z'\cot\alpha)/d_1,$$

$$\cos\psi_4\cos\psi_5 = 4zz'(\cos\alpha/d_2)^2,$$

and the local-area-specific energy profiles can be obtained through integration over the photon wavelengths. The profiles of the spectral local-area-specific rate of energy incidence on the corrugated plates were directly calculated from Eq. 1. However, none of these equations could be used directly to determine the LASREA, due to the absorption of the photons reflected from the conjugate wings. A procedure was implemented to consider the absorption of reflected photons while calculating the LASREA of the corrugated plates (see the section in the Appendix on the procedure for calculating the LASREA). This procedure involves iteration on expressions based on Eqs. 1 through 4. The preceding equations were solved numerically using Simpson's method (Rice and Do, 1995). Selected calculation results are presented and discussed in the next section.

Simulation Results and Discussions

Figures 3 through 9 show the calculated typical radiation fields on the TiO_2-coated corrugated plates in regions away

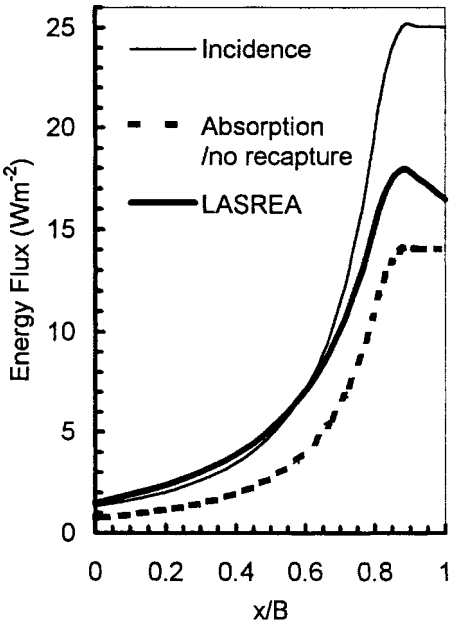

Figure 3. Radiation field on the surface of a lamp-illuminated corrugated plate (angle = 10°), where $x/B = 1$ is closest to the radiation source.

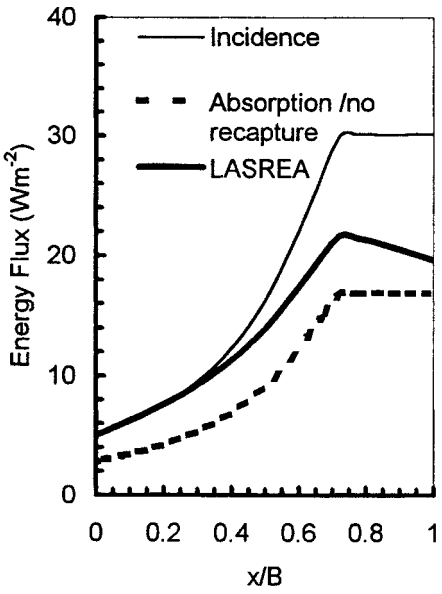

Figure 4. Radiation field on the surface of a lamp-illuminated corrugated plate (angle = 20°), where $x/B = 1$ is closest to the radiation source.

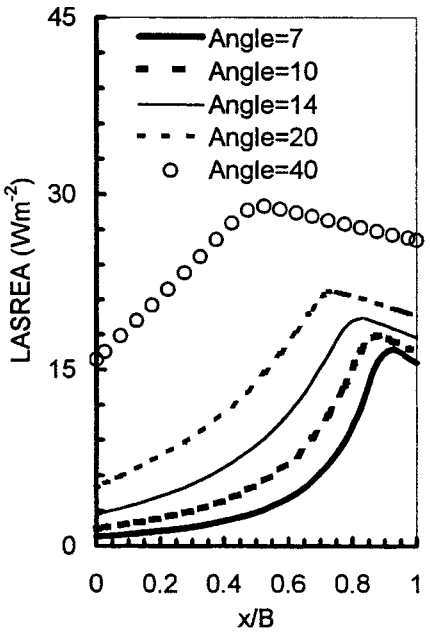

Figure 6. Comparison of the LASREA on the surfaces of lamp-illuminated corrugated plates with different angles (given in degrees).

from the ends, where the end effects were shown to be insignificant. The radiation fields of lamp-illuminated corrugated plates are plotted in Figures 3 through 6, while those of the solar-illuminated plates are given in Figures 7 through 9. The keys to these figures include:

- *Incidence:* the local-area-specific rate of energy incidence (calculated with Eq. 1 for the lamp-illuminated case).
- *Absorption/no recapture:* the local-area-specific rate of energy absorption if no reflected photon could be captured (calculated with Eqs. 1 and 2 for the lamp-illuminated case).
- *LASREA:* the local-area-specific rate of energy absorption, including the effect of recapturing reflected photons (calculated with the procedure described in the Appendix).

It can be seen from these figures that the radiation fields due to solar radiation are much more uniform than those due to lamp radiation. This occurs mainly because of the contri-

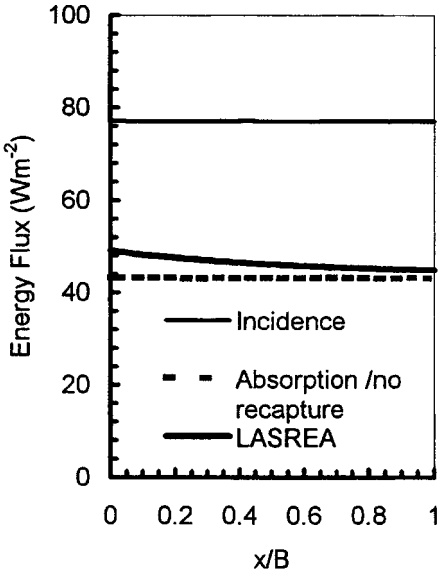

Figure 5. Predicted incidence on the surface of a corrugated plate with angle = 97.5°.

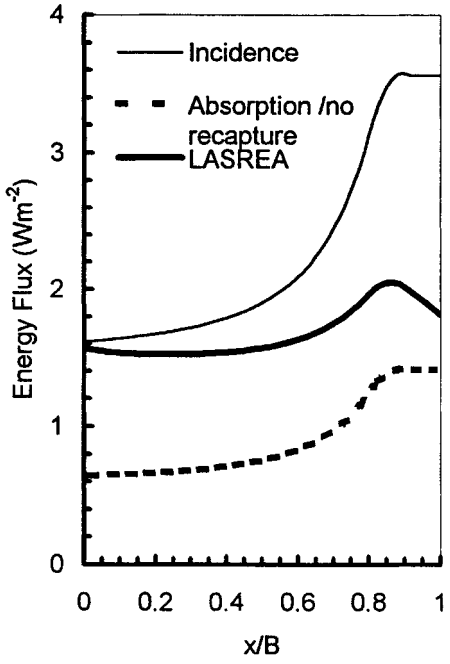

Figure 7. Radiation field on the surface of a solar-illuminated corrugated plate (angle = 10°).

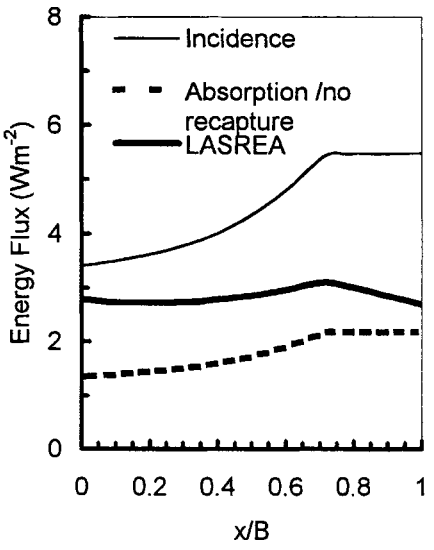

Figure 8. Radiation field on the surface of a solar-illuminated corrugated plate (angle = 20°).

bution of the direct parallel fraction, which was assumed to be normal to the reactor cover in these simulations. Since photocatalytic reactions typically follow lower-order dependency (usually between 0.5 and 1) on radiation intensity (Parent et al., 1996), a uniform LASREA results in higher energy efficiency if the system is not limited by mass transfer.

Several observations can be obtained from the results shown in Figures 3, 4, 7 and 8. For the same radiation intensity on the lamp sleeve, the LASREA profiles of the corrugated plates are dependent on the angles of these corrugations. By comparing the ''absorption/no recapture'' and the ''LASREA'' curves in these figures, we can easily note the significance of the recapture of the reflected photons. This is particularly noticeable in Figure 3, where the surfaces deeper within the corrugation ($x/B < 0.5$) have a LASREA greater than the direct incident energy reaching the surface from the radiation source. The corrugations tend to ''funnel'' reflected photons onto the deeper surfaces, where direct illumination is more limited. In addition, since photons tend not to be reflected out of the reactor, the energy absorption efficiency (that is, absorbed/incident energy) is significantly improved. This enhancement is again a strong function of the angle of the corrugated plates (Figures 3 vs. 4, 7 vs. 8).

As indicated in Figures 3, 4, 7 and 8, regions exist (that is, x/B close to 1) on the corrugated plates in which (these regions) uniform incidence is predicted. The extent of this region is dependent on the angle of a corrugated plate, but not on the radiation source used (Figure 3 vs. 7 and Figures 4 vs. 8). This phenomenon is attributed to the effect of refraction on the phase interfaces at both sides of the lamp sleeve. Based on Snell's law, the maximum angle of refraction (with respect to the norm of the lamp sleeve) after the UV rays penetrate the lamp sleeve/liquid interface can be calculated to be 48.75° [that is, $\arcsin(n_a/n_w)$]. Therefore, when the angle of a corrugated plate is greater than 97.5°, the incidence on the whole surface should be uniform regardless of the radiation patterns (that is, spherical, diffuse, direct parallel, or combinations) of the radiation source. This hypothesis is confirmed by the results depicted in Figure 5.

Figures 6 and 9 show the combined LASREA results for lamp and solar illuminated reactors, respectively. While the previous figures suggest that a small angle could result in a high-energy absorption efficiency, it is seen here that they also have a less uniform LASREA. Also, the smaller angles have a lower average area-specific rate of energy absorption, due to the smaller ''window'' open to illumination (that is, lamp sleeve in Figure 2b).

The effect of the angle of the corrugated plates on the energy absorption efficiency is depicted in Figure 10, where it

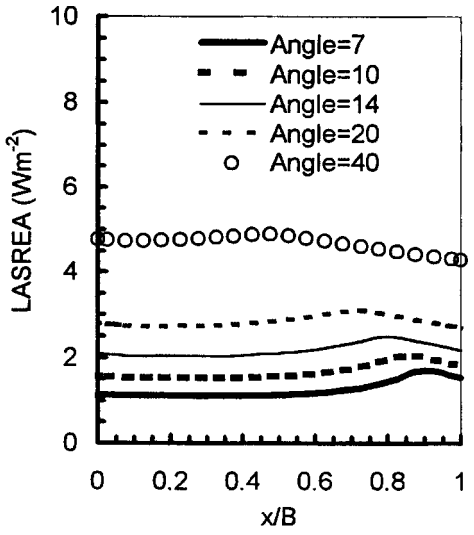

Figure 9. Comparison of the LASREA on the surfaces of solar-illuminated corrugated plates with different angles (in deg).

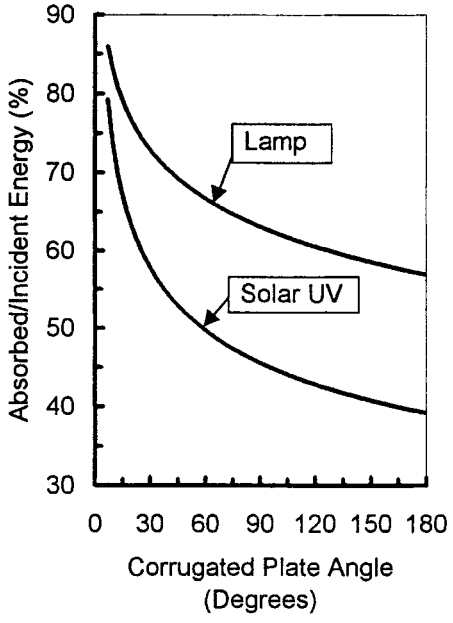

Figure 10. Effect of photon recapture on the radiation absorption efficiency of the TiO_2-coated corrugated plates.

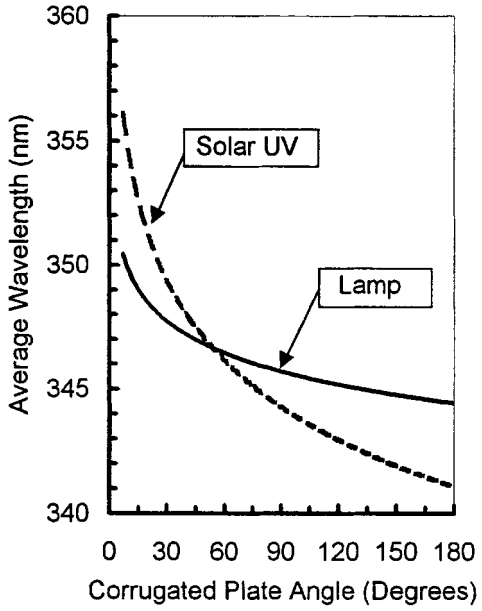

Figure 11. Effect of recapture on the average wavelength of the photons absorbed by TiO_2-coated corrugated plates.

can be seen that most of the radiative energy incident on a flat plate catalyst film (angle of 180°) will be reflected out of the reactor and dissipated as waste. This dissipation is more severe when the reactor is illuminated with sunlight, since the abundance of longer wavelength UV photons is not easily absorbed (see Figures A1 and A2 in the Appendix). In comparison, the corrugated plate can enhance the energy absorption efficiency of the solar UV by more than 100%. The corresponding enhancement for a lamp-illuminated system was calculated to be approximately 50%.

The average wavelength of the absorbed photons could be calculated using the integration shown in Equation A35 in the Appendix, and this is shown in Figure 11 for a range of corrugation angles. In this case, the wavelength is averaged based on the absorbed energy rather than a number average based on quantities of photons. It is apparent from this plot that the flat-plate geometry (angle 180°) can only effectively absorb the shorter wavelength photons. Longer wavelength photons, which are still photocatalytically active, are captured more easily by the corrugated-plate geometries. Again, the effect is more pronounced for solar illumination, due to the abundance of longer wavelength photons. Based on these two plots, we can also confirm that the radiation field is more sensitive to the angle of the corrugated plate when it is smaller than 30°.

Conclusions

Radiation fields on TiO_2-coated corrugated plates were modeled based on first principles. A new term, the local-area-specific rate of energy absorption (LASREA), was adopted to describe the radiation fields in such heterogeneous photoreactors.

Recapture of the reflected photons was considered in the model and was found to result in higher photon absorption efficiency as well as more uniform LASREA, which was shown to depend strongly on the angle of the corrugated plates. Compared to a flat plate, one corrugated plate was predicted to enhance the energy absorption efficiency by more than 100% for solar UV radiation and 50% for rays from UV-A fluorescent lamps. The difference in this enhancement is due to the different radiation patterns (that is, direct parallel vs. diffuse) and the different spectral distributions of these two types of radiation sources. The profiles of the LASREA on solar-powered corrugated plates were found to be more uniform than those powered by UV-A fluorescent lamps.

The angle of the corrugated plate has profound effects on the LASREA and the energy absorption efficiency. The smaller the angle, the higher the energy absorption efficiency, but the less uniform the LASREA on catalyst films. The smaller the angle, the lower the average area-specific rates of photon absorption due to the reduced area of exposure to the lamp sleeve. The radiation field is most sensitive to the angles smaller than 30°.

The LASREA concept described here can be applied to optimize other details of the reactor design, such as the corrugation depth and lamp spacing, or to predict the effects of varying solar positions. It can also be applied to other reactor geometries that seek to maximize the recapture of reflected photons.

Acknowledgments

Financial support for this work was provided by the Natural Sciences and Engineering Research Council of Canada. Z. Zhang was the holder of an Ontario Graduate Scholarship during part of this work.

Notation

fn_λ = fraction of the UV energy that penetrates a 0.25-in. Plexiglas G-UVT, as a function of photon wavelength, dimensionless
k_3 = extinction coefficient of Plexiglas G-UVT^{-1}
n_a, n_w, n_s = refractive indexes of the air, the reaction medium, and the lamp sleeve
x, y, z = rectangular Cartesian coordinate, m
α = half-angle of the corrugated plate, degrees
δ = thickness of the lamp sleeve, $\delta = 0.00635$ m
ψ_w = solid angles with respect to the normal of the lamp sleeve at the water side, Sr

Subscripts and Superscripts

w = reaction medium
n = after penetrating lamp sleeve
w = reaction medium side of the reaction medium/lamp sleeve phase interface

Literature Cited

Aguado, M. A., J. Giménez, and S. Cervera-March, "Continuous Photocatalytic Treatment of Cr(VI) Effluents with Semiconductor Powders," *Chem. Eng. Commun.*, **104**, 71 (1991).

Alfano, O. M., R. L. Romero, and A. E. Cassano, "Radiation Field Modeling in Photoreactors—1: Homogeneous Media; 2. Heterogeneous Media," *Chem. Eng. Sci.*, **41**, 421, 1137 (1986).

Belhacova, L., J. Krysa, and J. Jirkovsky, "Inactivation of Microorganisms in a Flow-Through Photoreactor with an Immobilized TiO_2 Layer," *J. Chem. Technol. Biotechnol.*, **74**, 149 (1999).

Bolduc, L., and W. A. Anderson, "Enhancement of the Biodegradability of Model Wastewater Containing Recalcitrant and In-

hibitory Chemical Compounds by Photocatalytic Pre-oxidation,'' *Biodegradation,* **8**, 237 (1997).
Cabrera, M. I., O. M. Alfano, and A. E. Cassano, ''Novel Reactor for Photocatalytic Kinetic Studies,'' *Ind. Eng. Chem. Res.*, **33**, 3031 (1994).
Cassano, A. E., C. A. Martín, R. J. Brandi, and O. M. Alfano, ''Photoreactor Analysis and Design: Fundamentals and Applications,'' *Ind. Eng. Chem. Res.*, **34**, 2155 (1995).
Crittenden, J. C., Y. Zhang, D. W. Hand, and D. L. Perram, ''Destruction of Organic Compounds in Water Use Supported Photocatalysts,'' *J. Solar Energy Eng.*, **118**, 123 (1996).
Curcó, D., S. Malato, J. Blanco, and J. Giménez, ''Photocatalysis and Radiation Absorption in a Solar Plant,'' *Solar Energy Mater. Solar Cells*, **44**, 199 (1996).
Goswami, D. Y., ''A Review of Engineering Developments of Aqueous Phase Solar Photocatalytic Detoxification and Disinfection Processes,'' *J. Solar Energy Eng.*, **119**, 101 (1997).
Holden, W., A. Marcellino, D. Valic, and A. C. Weedon, ''Titanium Dioxide Mediated Photochemical Destruction of Tricholoethylene Vapors in Air,'' *Photocatalytic Purification and Treatment of Water and Air*, D. F. Ollis and H. Al-Ekabi, eds., Elsevier, Amsterdam, p. 393 (1993).
Lawton, L. A., P. K. J. Robertson, and M. Jaspars, ''Detoxification of Microcystins Using TiO_2 Photocatalytic Oxidation,'' *Environ. Sci. Technol.*, **33**, 771 (1999).
Lin, W. Y., and K. Rajeshwar, ''Photocatalytic Removal of Nickel from Aqueous Solutions Using Ultraviolet-Irradiated TiO_2,'' *J. Electrochem. Soc.*, **144**, 2751 (1997).
Marinangeli, R. E., and D. F. Ollis, ''Photo-Assisted Heterogeneous Catalysis with Optical Fibres: I. Isolated Single Fibre,'' *AIChE J.*, **23**, 415 (1977).
Matthews, R. W., ''Photooxidation of Organic Impurities in Water Using Thin Films of Titanium Dioxide,'' *J. Phys. Chem.*, **91**, 3328 (1987).
Mehos, M. S., and C. S. Turchi, ''Field Testing Solar Photocatalytic Detoxification on TCE-Contaminated Groundwater,'' *Environ. Prog.*, **12**, 194 (1993).
Parent, Y., D. Blake, B. K. Magrini, C. Lyons, C. Turchi, A. Watt, E. Wolfrum, and M. Prairie, ''Solar Photocatalytic Processes for the Purification of Water: State of Development and Barriers to Commercialization,'' *Solar Energy*, **56**, 429 (1996).
Pasquali, M., F. Santarelli, J. F. Porter, and P. L. Yue, ''Radiative Transfer in Photocatalytic Systems,'' *AIChE J.*, **42**, 532 (1996).
Philips Lighting Company, *Specialty Catalog*, Sommerset, NJ (1998).
Rice, R. G., and D. D. Do, *Applied Mathematics and Modeling for Chemical Engineers*, Wiley, New York (1995).
Rizzuti, L., ''Absorption of Light Energy in Photoreactors,'' *Photoelectrochemistry, Photocatalysis, and Photoreactors*, M. Schiavello, ed., Reidel, Dordrecht, The Netherlands, p. 587 (1985).
Roger, M., and J. Villermaux, ''Modeling of Light Absorption in Photoreactors: 1. General Formulation Based on the Laws of Photometry,'' *Chem. Eng. J.*, **17**, 219 (1979).
Romero, R. L., O. M. Alfano, and A. E. Cassano, ''Cylindrical Photocatalytic Reactors: Radiation Absorption and Scattering Effects Produced by Suspended Fine Particles in an Annular Space,'' *Ind. Eng. Chem. Res.*, **36**, 3094 (1997).
Turchi, C. S., and M. S. Mehos, ''Solar Photocatalytic Detoxification of Groundwater: Developments in Reactor Design,'' *Chem. Oxid.*, **2**, 301 (1994).
U.S. Precision Lens, *The Handbook of Plastic Optics*, U.S. Precision Lens, Cincinnati, OH (1973).
Zhang, Z., ''Analysis of a Corrugated Plate Photocatalytic Reactor,'' *PhD Thesis, Univ. of Waterloo, Waterloo, Ont., Canada* (1999).

Appendix: Model Development

Calculation of the spectral specific irradiance

Lamp Radiation. Figure A1 shows the manufacturer's data for the relative spectral irradiance of the fluorescent lamps assumed in this study. As shown in this figure, a normal distribution function ($\sigma = 15.75$ nm, $\lambda_{avg} = 353$ nm) was found to fit these data quite well. The lamps were arranged such that the UV-A reading of the radiometer was constant (let it be w) over the surface of the entire outer surface lamp sleeve. Therefore, the spectral irradiance at any point on the outer surface of the lamp sleeve can be expressed with:

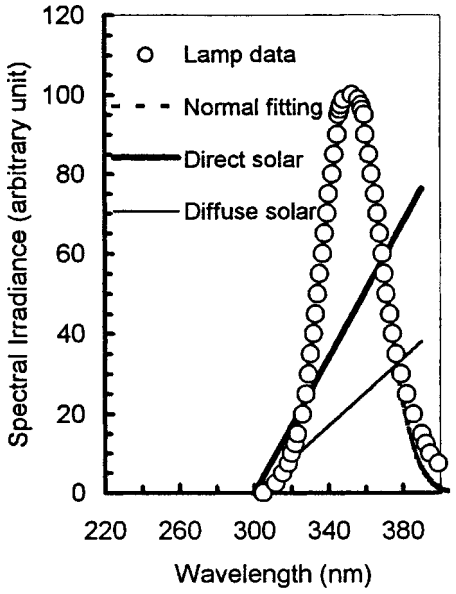

Figure A1. Spectral irradiance of fluorescent lamp (based on Philips TLK 40W/10R) and solar UV.

$$w_\lambda = \frac{w}{\sqrt{2\pi}\,\sigma}\exp\left(-\frac{(\lambda-353)^2}{2\sigma^2}\right). \tag{A1}$$

Based on a radiation energy balance over a unit hemisphere and Eq. A1, the spectral specific irradiance at any point of the air side of the lamp sleeve can be written as

$$w^{\alpha}_{\lambda\psi} = \frac{w_\lambda}{\pi}\cos\psi_a = \frac{w\cos\psi_a}{\pi\sqrt{2\pi}\,\sigma}\exp\left(-\frac{(\lambda-353)^2}{2\sigma^2}\right). \tag{A2}$$

Solar Radiation. Based on Assumption 2, the spectral specific irradiance due to the direct parallel fraction of the solar UV was derived through an energy balance. The result can be expressed as:

$$w^{p}_{\lambda\psi} = \begin{cases} 4.884\times10^{-3}(\lambda-300) & \text{for } \psi_a = 0 \\ 0 & \text{for } \psi_a \neq 0. \end{cases} \tag{A3}$$

The spectral specific irradiance of the diffuse solar UV was also derived using the same method, resulting in

$$w^{d}_{\lambda\psi} = \frac{2.442\times10^{-3}}{\pi}(\lambda-300)\cos\psi. \tag{A4}$$

Spectral extinction coefficient of the lamp sleeve

If a UV ray is incident on the lamp sleeve at an angle of ψ_a, its angles of refraction after penetrating the air/solid and solid/liquid interfaces, ψ_s and ψ_w, are calculated based on Snell's law:

$$n_a \sin \psi_a = n_s \sin \psi_s = n_w \sin \psi_w. \quad \text{(A5)}$$

Based on an energy balance over a unit hemisphere, we derive:

$$fn_\lambda w_\lambda = \int_0^{\pi/2} 2\pi \sin \psi \, w_{\lambda\psi} \exp\left(- \frac{\delta k_3}{\sqrt{1-(n_a/n_s \sin \psi)^2}} \right) d\psi, \quad \text{(A6)}$$

which gives the extinction coefficient of the lamp sleeve as a function of photon wavelength.

The spectral transmission information, fn_λ from the plastic supplier, can therefore be used to calculate the spectral extinction coefficient, k_3, through Eq. A7 below. The extinction coefficient as a function of wavelength was obtained by numerically solving Eq. A7 with Maple V. The results are presented in Figure A2:

$$fn_\lambda = \int_0^{\pi/2} \exp\left(- \frac{\delta k_3}{\sqrt{1-(n_a/n_s \sin \psi)^2}} \right) \sin 2\psi \, d\psi. \quad \text{(A7)}$$

Effect of refraction on radiation pattern

As a result of refraction on the phase interface, the original radiation pattern will not usually be preserved when light travels from one medium to another. The radiation pattern

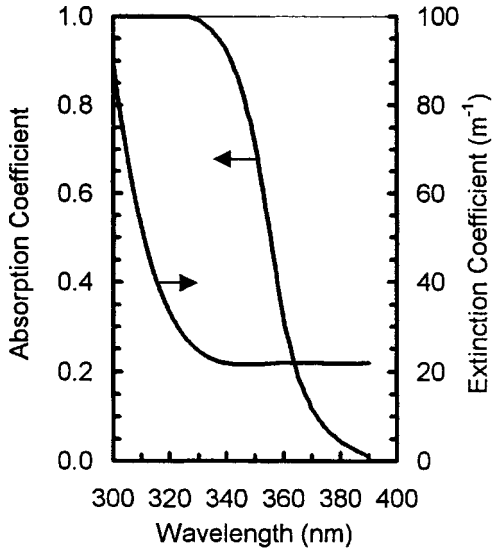

Figure A2. Absorption coefficient of the TiO_2 film (Crittenden et al., 1995) and calculated extinction coefficient of the acrylic lamp sleeve.

in the second medium can be determined based on Snell's law and energy balances on the phase interface. For example, an energy balance on the air/lamp sleeve and lamp sleeve/reaction medium interfaces requires that:

$$w^a_{\lambda\psi} 2\pi \sin \psi_a d\psi_a = w^s_{\lambda\psi} 2\pi \sin \psi_s d\psi_s = w^w_{\lambda\psi} \exp(k_3 \delta / \cos \psi_s) 2\pi \sin \psi_w d\psi_w. \quad \text{(A8)}$$

By taking derivatives with respect to the solid angles, we can obtain from Eq. A5:

$$n_a \cos \psi_a d\psi_a = n_s \cos \psi_s d\psi_s = n_w \cos \psi_w d\psi_w.$$

Combining this equation and Eqs. A2, A5 and A8, we derive

$$w^s_{\lambda\psi} = \left(\frac{n_s}{n_a} \right)^2 \frac{\cos \psi_s}{\cos \psi_a} w^a_{\lambda\psi} = \left(\frac{n_s}{n_a} \right)^2 \frac{w_\lambda}{\pi} \cos \psi_s.$$

The spectral specific irradiance at any point of the liquid side of the lamp sleeve/reaction medium interface can be derived in the same way. The result is

$$w^w_{\lambda\psi} = \left(\frac{n_w}{n_a} \right)^2 \frac{w_\lambda}{\pi} \cos \psi_w \exp^{(-k_3 \delta [1-(n_w/n_s \sin \psi_w)^2]^{-0.5})}. \quad \text{(A9)}$$

Radiation fields under lamp radiation

Equations A10 through A18 are obtained using analytical geometry. Under the coordinate system shown in Figure 2A, the upper wing of the corrugated plate can be expressed as

$$x - z \tan \alpha = 0, \quad \text{(A10)}$$

where $0 \le x \le B$ and $-L/2 \le y \le L/2$ and α is one-half of the angle indicated in Figure 2A. The lower wing can be expressed as

$$x + z \tan \alpha = 0, \quad \text{(A11)}$$

where $0 \le x \le B$ and $-L/2 \le y \le L/2$, and the lamp sleeve can be expressed as

$$x = B, \quad \text{(A12)}$$

where $-L/2 \le y \le L/2$ and $-B \tan \alpha \le z \le B \tan \alpha$.

For points $P(x', y', z')$ on the upper wing, $P''(x'', y'', z'')$ on the lower wing, and $P(x, y, z)$ on the lamp sleeve, the square of the distance from P to P' can be expressed as

$$d_1^2 = (z' \cot \alpha - B)^2 + (y' - y)^2 + (z' - z)^2, \quad \text{(A13)}$$

and the square of the distance from P'' to P' can be expressed as

$$d_2^2 = (\cot \alpha)^2 (z' + z'')^2 + (y' - y'')^2 + (z' - z'')^2. \quad \text{(A14)}$$

The cosine of the angle between the normal of the lamp sleeve and line PP' can be expressed as

$$\cos\psi_w = (B - z'\cot\alpha)/d_1, \tag{A15}$$

and the cosine of the angle between the normal of the upper wing and line PP' can be written as

$$\cos\psi_1 = \sin\alpha(B - z\cot\alpha)/d_1. \tag{A16}$$

The cosine of the angle between the normal of the lower wing and line $P''P'$ can be expressed as

$$\cos\psi_4 = 2z'\cos\alpha/d_2, \tag{A17}$$

and the cosine of the angle between the normal of the upper wing and line $P''P'$ can be written as

$$\cos\psi_5 = 2z''\cos\alpha/d_2. \tag{A18}$$

Based on the principles of geometric optics, the spectral local-area-specific rate of energy incidence on point $P(x', y', z')$, due to the radiation from the lamp sleeve, can be written as

$$I_u^s(y', z') = \frac{w_\lambda}{\pi}\left(\frac{n_w}{n_a}\right)^2 \iint_{S1} \frac{\cos\psi_1}{d_1^2}\cos\psi_w \times \exp^{(-k_3\delta[1-((n_w/n_s)\sin\psi_w)^2]^{-0.5}-k_4 d_1)}dy\,dz. \tag{A19}$$

The integration is over surface $S1: n_w/n_a \sin\psi_w \le 1$.

Within the wavelength range in question, the extinction coefficient in the reaction medium, k_4, was assumed to be zero.

If the photons reflected from the lower wing could be ignored, the relationship between the incident and absorbed energy at wavelength λ could then be expressed by Eq. A20:

$$q_u(y', z') = a(\lambda) I_u(y', z'). \tag{A20}$$

As a result of the absorption of the photons reflected from the lower wing, neither Eq. A19 nor Eq. A20 give the LASREA on the upper wing. In order to calculate the LASREA, an additional procedure was developed and is presented in the section titled ''Procedure for the Calculation of the LASREA.''

Radiation field under solar radiation

Contributions from the diffuse fraction of the solar UV can be modeled using the equations in the preceding section, except that $w_{\lambda\psi}^d$ from Eq. A4 should be used instead of $w_{\lambda\psi}$ from Eq. A2.

Based on geometric optics, the spectral local-area-specific rate of energy incidence on point $P(x', y', z')$, due to the direct parallel fraction of the solar UV from the lamp sleeve, has been derived to be

$$I_\lambda^p = w_{\lambda\psi}^p \sin\alpha \exp^{(-k_3\delta)}. \tag{A21}$$

This equation holds for both corrugated and flat ($\alpha = 90°$) plates.

Procedure for the Calculation of the LASREA

Step 1. Imagine at time t photons have just contacted the two wings of the corrugated plate from the lamp sleeve and no reflection has occurred yet. The spectral local-area-specific rate of energy incidence at any location of the upper wing [that is, $I_u^s(y', x')$] can be calculated from Eqs. A5, A13, A15, A16 and A19. Let

$$I_u^{(0)}(y', z') = I_u^s(y', z') \tag{A22}$$

and

$$q_u^{(0)}(y', z') = a(\lambda) I_u^{(0)}(y', z'). \tag{A23}$$

Since the radiation field of the upper and lower wings of the corrugated plate are symmetric to plane $z = 0$,

$$I_l^{(0)}(y', z') = I_u^{(0)}(y', -z'). \tag{A24}$$

Step 2. Imagine at time $t + \Delta t$ photons on the two wings of the corrugated plate just finished their first reflection (to conjugate wing and to lamp sleeve). The spectral local-area-specific rate of energy incidence at any location of the upper wing due to this reflection can be calculated based on:

$$I_u^{(1)}(y', z') = \frac{[1 - a(\lambda)]}{\pi}\iint_l \frac{I_u^{(0)}(y, -z)\cos\psi_4\cos\psi_5}{d_2^2} \times \exp^{(-k_4 d_2)}dy\,dz. \tag{A25}$$

The fraction that is absorbed is

$$q_u^{(1)}(y', z') = a(\lambda) I_u^{(1)}(y', z'). \tag{A26}$$

Since the radiation field of the upper and lower wings of the corrugated plate are symmetric to plane $z = 0$,

$$I_l^{(1)}(y', z') = I_u^{(1)}(y', -z'). \tag{A27}$$

Step 3. Imagine at time $t + 2\Delta t$ photons on the two wings of the corrugated plate just finished their second reflection (to conjugate wing and to lamp sleeve). The spectral local-area-specific rate of energy incidence at any location of the upper wing due to this reflection can be calculated based on

$$I_u^{(2)}(y', z') = \frac{[1 - a(\lambda)]}{\pi}\iint_l \frac{I_u^{(1)}(y, -z)\cos\psi_4\cos\psi_5}{d_2^2} \times \exp^{(-k_4 d_2)}dy\,dz. \tag{A28}$$

The absorbed part can be calculated using

$$q_u^{(2)}(y', z') = a(\lambda) I_u^{(2)}(y', z'). \quad \text{(A29)}$$

Since the radiation field of the upper and lower wings of the corrugated plate are symmetric to plane $z = 0$,

$$I_l^{(2)}(y', z') = I_u^{(2)}(y', -z'). \quad \text{(A30)}$$

Step (n + 1). Imagine at time $t + n\Delta t$ photons on the two wings of the corrugated plate just finished their nth reflection (to conjugate wing and to lamp sleeve). The spectral local-area-specific rate of energy incidence at any location of the upper wing due to this reflection can be calculated based on:

$$I_u^{(n)}(y', z') = \frac{[1 - a(\lambda)]}{\pi} \int\int_l \frac{I_u^{(n-1)}(y, -z) \cos\psi_4 \cos\psi_5}{d_2^2} \times \exp^{(-k_4 d_2)} dy\, dz. \quad \text{(A31)}$$

The absorbed part can be calculated using

$$q_u^{(n)}(y', z') = a(\lambda) I_u^{(n)}(y', z'). \quad \text{(A32)}$$

Since the radiation field of the upper and lower wings of the corrugated plate are symmetric to plane $z = 0$,

$$I_l^{(n)}(y', z') = I_u^{(n)}(y', -z'). \quad \text{(A33)}$$

After a sufficient number of reflections, the calculation is stopped based on the criterion,

$$I_u^{(n)}(y', z') \le 0.01 \times I_u^{(1)}(y', z'). \quad \text{(A34)}$$

Given the speed at which the photons travel, Δt could actually be considered to be infinitely small. The LASREA can therefore be calculated with:

$$Q_u(y', z') = Q_l(y', -z') = \int_\lambda \left\{ q_u^{(0)}(y', z') + q_u^{(1)}(y', z') + \ldots + q_u^{(n)}(y', z') \right\} d\lambda, \quad \text{(A35)}$$

where n is selected based on the stopping criterion given above in Eq. A34.

Manuscript received July, 1999, and revision received Feb. 4, 2000.